ResearchGate

See discussions, stats, and author profiles for this publication at: https://www.researchgate.net/publication/232247115

Molecular geometry, vibrational spectra, atomic charges, frontier molecular orbital and Fukui function analysis of antiviral drug zidovudine

ARTICLE *in* SPECTROCHIMICA ACTA PART A MOLECULAR AND BIOMOLECULAR SPECTROSCOPY · SEPTEMBER 2012

Impact Factor: 2.35 · DOI: 10.1016/j.saa.2012.09.018 · Source: PubMed

CITATIONS
3

READS
70

4 AUTHORS, INCLUDING:

Srinivasan S
Presidency College
33 PUBLICATIONS **128** CITATIONS
SEE PROFILE

T.J. Bhoopathy
Pachaiyappa's College, Chennai
8 PUBLICATIONS **11** CITATIONS
SEE PROFILE

Sethu Gunasekaran
St. Peter's University
221 PUBLICATIONS **1,270** CITATIONS
SEE PROFILE

All in-text references underlined in blue are linked to publications on ResearchGate, letting you access and read them immediately.

Available from: Sethu Gunasekaran
Retrieved on: 27 January 2016

Spectrochimica Acta Part A: Molecular and Biomolecular Spectroscopy 99 (2012) 189–195

Contents lists available at SciVerse ScienceDirect

Spectrochimica Acta Part A: Molecular and Biomolecular Spectroscopy

journal homepage: www.elsevier.com/locate/saa

Molecular geometry, vibrational spectra, atomic charges, frontier molecular orbital and Fukui function analysis of antiviral drug zidovudine

G.R. Ramkumaar [a], S. Srinivasan [b,*], T.J. Bhoopathy [a], S. Gunasekaran [a]

[a] PG and Research Department of Physics, Pachaiyappa's College, Chennai 600 030, TN, India
[b] PG and Research Department of Physics, Presidency College, Chennai 600 005, TN, India

HIGHLIGHTS

- The solid phase FTIR and FT-Raman spectra of AZT were recorded and analyzed.
- The optimized geometry and vibrational wavenumbers were computed using ab initio HF and DFT methods.
- The complete vibrational assignment and spectroscopic analysis have been carried out.
- The DFT calculated HOMO and LUMO energies show that charge transfer occurs within molecule.
- The Fukui functions were calculated to explain the chemical selectivity or reactivity site in AZT.

GRAPHICAL ABSTRACT

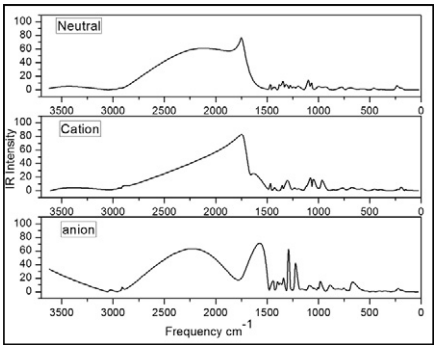

ARTICLE INFO

Article history:
Received 14 August 2012
Accepted 9 September 2012
Available online 23 September 2012

Keywords:
Zidovudine
FTIR
FT-Raman
Density functional theory

ABSTRACT

The solid phase FT-IR and FT-Raman spectra of zidovudine (AZT) were recorded in the regions 4000–400 and 3500–100 cm^{-1}, respectively. The optimized geometry, frequency and intensity of the vibrational bands of zidovudine were obtained by the Restricted Hartree–Fock (RHF) density functional theory (DFT) with complete relaxation in the potential energy surface using 6-31G(d,p) basis set. The harmonic vibrational frequencies for zidovudine were calculated and the scaled values have been compared with experimental values of FTIR and FT-Raman spectra. The observed and the calculated frequencies are found to be in good agreement. The harmonic vibrational wave numbers and intensities of vibrational bands of zidovudine with its cation and anion were calculated and compared with the neutral AZT. The DFT calculated HOMO and LUMO energies shows that charge transfer occurs within the molecule. The electron density-based local reactivity descriptors such as Fukui functions were calculated to explain the chemical selectivity or reactivity site in AZT.

© 2012 Elsevier B.V. All rights reserved.

Introduction

Human Immunodeficiency Virus (HIV) is the causative agent of the pandemic disease Acquired Immune Deficiency Syndrome (AIDS). HIV acts to disrupt the immune system which makes the body susceptible to opportunistic infections. Twenty years of research by countless scientists around the world has led to the discovery and exploitation of several targets in the replication cycle of HIV. Many lives have been saved, prolonged and improved as a result of this massive effort. In particularly successful target has been the inhibition of HIV protease. In combination with the inhibition of HIV reverse transcriptase, protease inhibitors have helped to reduce viral loads and partially restore the immune system. Unfortunately, viral mutations leading to drug resistance and harmful side effects of the current medicines have identified the need for new

* Corresponding author. Tel.: +91 9884766203.
E-mail address: dr_s_srinivasan@yahoo.com (S. Srinivasan).

1386-1425/$ - see front matter © 2012 Elsevier B.V. All rights reserved.
http://dx.doi.org/10.1016/j.saa.2012.09.018

drugs to combat HIV. Zidovudine, 3-azido-3-deoxythymidine (AZT), is an organic compound used to delay the development of Acquired Immune Deficiency Syndrome (AIDS) in patients infected with HIV, to reduce mother-to child HIV transmission and as radio sensitizer in cancer radiotherapy, because it is a telomerase inhibitor with potential anticancer properties [1]. Jerome Horowitz first synthesized AZT in the year 1964 [2]. In the solid state AZT forms a hydrogen bond network [3].

In spite of its importance for pharmaceutical purposes, however, the reported spectroscopic studies on zidovudine are scarce. Cheng et al. [4] investigated different conformers of AZT by simulating their IR spectra. Improper hydrogen bonds caused blue shift in C—H bond stretch vibrations in three conformers of zidovudine that have been studied using DFT in gas phase and in aqueous solution. Recently, Peepliwal et al. [5] developed and then validated two analytical methods for the quantification of AZT containing solid dosage form by using FTIR and UV–Vis spectroscopy. Nayak et al. [6] studied the sustained release of AZT using chitosan as a polymer matrix by applying IR spectroscopy and differential scanning calorimetry (DSC). They have demonstrated the stability of the drug during the encapsulation process and have shown more than 95% drug release in 12 h. Rivas et al. [7,8] used normal Raman as well as SERS to carry out a structural study of AZT in solid state, aqueous solution and when adsorbed on silver nanoparticles prepared by reduction with citrate. Raviolo et al. [9] investigated X-ray crystal and molecular structure, NMR, IR and Raman spectra, the thermal behavior of a novel carbonate of AZT and its lipophilic properties in order to enhance pharmacological effects. A study concerning the biodegradation of AZT in the environment was carried out by Kruszewska et al. [10] using chromatographic methods, mass analyses, NMR and vibrational methods. A scan of literature survey reveals that to the best of our knowledge, no DFT studies on vibrational spectroscopic studies of AZT and its cationic and anionic forms have been reported so far. Also the molecular orbital analysis and chemical reactivity of the title molecule AZT have not been reported till date via both experimentally or theoretically. Hence, in this study, DFT calculations were used for a proper investigation of the structure and vibrational and electronic properties of AZT in its neutral and cationic and anionic forms.

Experimental

The compound zidovudine in the light white powder form as obtained from Sigma–Aldrich chemical company, with stated purity of greater than 99% and it was used as such without further purification. The FTIR spectrum of this compound was recorded in the region 4000–400 cm^{-1} in evacuation mode on Nexus 670 DTGS using KBr pellet technique (solid phase) with 4.0 cm^{-1} resolution. The FT-Raman spectrum was recorded using 1064 nm line of Nd: YAG laser as excitation wavelength in the region 3500–100 cm^{-1} on Bruker IFS 66 V spectrometer equipped with FRA 106 Raman module was used as an accessory.

Computational details

The DFT calculations are performed on a Pentium IV personal computer using the Gaussian-03W program package [11]. The geometries are optimized in 6-31G(d,p) basis sets using Restricted Hartree Fock (RHF) and density functional theory employing the B3LYP keyword, which invokes Becke's three parameter hybrid method [12] using the correlation function of Lee et al. [13]. Since the molecule possesses amino and nitro groups, we used diffuse and polarization functions for better description of these bonds. The optimized geometrical structures were utilized in the calculations of harmonic vibrational wave numbers to characterize all stationary points as minima.

Results and discussion

AZT and its positive and negative ions are subjected to geometry optimizations in their ground state. For each method, geometry optimizations are performed. The requested convergence on the maximum density matrix was 10^{-6} a.u.; the threshold value of the maximum displacement is 0.0018 Å and that of the maximum force is 0.00045 Hartree/Bohr using the Berny analytical gradient optimization routine [14,15]. The nature of stationary points is checked by diagonalizing the Hessian matrix to determine the number of imaginary frequencies (zero for local minimum). The self consistent field (SCF) energy of AZT at B3LYP level with the basis sets 6-31G(d,p) and 6-31G++(d,p) is found to be −492.123 a.u. and −491.83 a.u. respectively and for its positive ion is found to be −492.146 a.u. and −491.844 a.u. respectively. The optimized structural parameters of AZT and its positive, negative ions is calculated by DFT levels with two different basis sets are listed in Table 1 in accordance with the atom numbering scheme given in Fig. 1. Table 1 also gives the bond length and bond angle difference (Δ) between neutral, positive and negative ions of AZT. The calculated bond distances and angles for the title compound are in agreement with experimental data.

Molecular geometry

The optimized molecular structure of the isolated AZT molecule are calculated using DFT and HF theory at 6-31G(d,p) level. Fig. 1 shows the optimized structure of AZT obtained from B3LYP and HF methods respectively, (atom numbering scheme adopted in the study). The optimized geometrical parameters are given in Table 1. The vibrationally averaged nuclear positions of AZT was used for harmonic vibrational frequency calculations. The global minimum energy obtained by DFT B3LYP and HF/6-31G(d,p) structure optimization for AZT are −963.52 a.u. and −957.92 a.u. respectively. The bond length between N_{17}—N_{18} was 1.236 Å was observed in B3LYP level and 1.229 Å in HF level, which is almost close to the bond length of 1.24 Å in an isolated N=N double bond. A triple bond character was observed for the terminal N_{18}—N_{19} bond with a bond distance of 1.102 Å by HF method, which agrees exactly with the experimental value of 1.10 Å. The azide bond angle N_{17}—N_{18}—N_{19} was 173° and 175.2° in B3LYP and HF levels respectively closely agree with the bond angle values reported by Chen et al. [16]. This azide bond angle value clearly indicates a non-linear asymmetric chain structure. Due to which a dihedral C_{13}—N_{17}—N_{18}—N_{19} bond angle becomes −176.1° and −175.3° in DFT and HF methods respectively as it was appended to a large unsymmetrical thymidine fragment. The pyrimidine and furan ring was non-planar. The carboxyl group (C_3=O_8) in the aromatic six membered ring shows the planar configuration with the dihedral angle of 179.9°, whereas another carboxyl group C_1=O_7 shows non-planar configuration with the dihedral angle of 177° was observed. The bond length of carboxyl group C_1—O_7 and C_3—O_8 confirms the double bond character. The breakdown of hexagonal symmetry of the benzene ring is obvious from the elongation of C_3—C_4 (1.463 Å) and contraction of C_4—C_5 (1.351 Å) from the normal value of 1.390 Å. The asymmetry of the benzene ring is also evident from the N_6—C_1—N_2 (113.9° in B3LYP and 114.7° in HF, C_3—C_4—C_5 (118.2° in B3LYP and 117.6° in HF and positive deviation of C_4—C_5—N_6 (124.6°) from the normal value of 120°. Comparing the bond length and bond angles of B3LYP with those of HF, as a whole the former are on the higher side than the latter and the B3LYP calculated values correlates well compared to those with the structurally related molecules. The slight variations in the molecular geometry prediction by the DFT method with the experimental data may be attributed to different environments of the molecule, being in the isolated state in the gas phase for theoretical

Table 1
Selected bond length (Å), bond angle (°) and dihedral angle (°) of AZT obtained from HF and B3LYP method with the basis set 6-31G(d,p).

Bond length	B3LYP	HF	Bond angle	B3LYP	HF	Dihedral angle	B3LYP	HF
R(1–2)	1.383	1.369	*A*(2–1–6)	113.9	114.7	*D*(6,1,2,3)	2.8	2.9
R(1–6)	1.399	1.377	*A*(2–1–7)	122.4	121.6	*D*(7,1,2,3)	−178.2	−178.1
R(1–7)	1.222	1.197	*A*(1–2–3)	128.8	128.3	*D*(2, 1,6,5)	−3.9	−4.5
R(2–3)	1.405	1.383	*A*(6–1–7)	123.8	123.7	*D*(2,1,6,11)	−176.5	−174.4
R(3–4)	1.463	1.466	*A*(1–6–5)	120.7	120.2	*D*(7,1,6,5)	177.0	176.5
R(3–8)	1.222	1.195	*A*(1–6–11)	119.6	119.8	*D*(7,1,6,11)	4.4	6.6
R(4–5)	1.351	1.329	*A*(2–3–4)	113.7	114.1	*D*(1,2,3,4)	−0.7	−0.3
R(4–9)	1.501	1.502	*A*(2–3–8)	120.7	120.7	*D*(1,2,3,8)	179.1	179.4
R(5–6)	1.387	1.386	*A*(4–3–8)	125.7	125.1	*D*(2,3,4,5)	−0.3	−0.5
R(6–11)	1.477	1.463	*A*(3–4–5)	118.2	117.6	*D*(2,3,4,9)	179.2	179.0
R(10–11)	1.413	1.390	*A*(3–4–9)	117.9	118.1	*D*(8,3,4,5)	179.9	179.6
R(10–14)	1.438	1.415	*A*(5–4–9)	123.8	124.3	*D*(8,3,4,9)	−0.6	−0.7
R(11–12)	1.544	1.535	*A*(4–5–6)	124.6	124.9	*D*(3,4,5,6)	−1.0	−1.2
R(12–13)	1.540	1.531	*A*(5–6–11)	119.3	119.2	*D*(9,4,5,6)	179.4	179.1
R(13–14)	1.536	1.528	*A*(6–11–10)	111.7	111.5	*D*(4,5,6,1)	3.4	4.0
R(13–17)	1.475	1.464	*A*(6–11–12)	115.0	115.6	*D*(4,5,6,11)	176.0	174.0
R(14–15)	1.515	1.510	*A*(11–10–14)	110.5	111.7	*D*(1,6,11,10)	65.7	63.2
R(15–16)	1.417	1.397	*A*(10–11–12)	107.4	107.1	*D*(1,6,11,12)	−57.0	−59.3
R(17–18)	1.236	1.229	*A*(10–14–13)	103.5	103.4	*D*(5,6,11,10)	−107.0	−106.7
R(18–19)	1.142	1.102	*A*(10–14–15)	109.7	109.7	*D*(5,6,11,12)	130.3	130.6
			A(11–12–13)	102.6	102.0	*D*(14,10,11,6)	−117.4	−121.2
			A(12–13–14)	102.1	101.8	*D*(14,10,11,12)	9.5	6.1
			A(12–13–17)	114.2	114.7	*D*(11,10,14,13	−29.7	−27.4
			A(14–13–17)	110.0	110.0	*D*(6,11,12,13)	139.5	142.5
			A(13–14–15)	114.0	114.1	*D*(10,11,12,13)	14.5	17.6
			A(13–17–18)	116.0	113.9	*D*(11,12,13,14)	−31.0	−32.5
			A(14–15–16)	108.6	108.7	*D*(11,12,13,17)	−149.8	−151.3
			A(17–18–19)	173.0	175.2	*D*(12,13,14,10)	37.2	36.8
						D(12,13,14,15)	156.3	155.9
						D(17,13,14,10)	158.9	158.9
						D(17,13,14,15)	−82.1	−81.9
						D(12,13,17,18)	−89.7	−88.0
						D(14,13,17,18)	156.1	157.9
						D(10,14,15,16)	−71.8	−71.0
						D(13,14,15,16)	172.8	173.4
						D(13,17,18,19)	−176.1	−175.3

R: bond distance; *A*: bond angle; *D*: dihedral angle.

study, whereas the experimental values of the molecule in the solid state thereby subjected to the intermolecular interactions. Although it has slight differences, calculated geometric parameters represent a good approximation, and they are the base for calculating other parameters.

Vibrational spectra

Infrared and Raman spectroscopic techniques provide important structural information making them a powerful molecular investigation tool. The molecule AZT as well as its cationic and anionic forms has 32 atoms. The SCF energy and geometrical parameters of AZT and its charged species in C_1 symmetry has lower values rather in C_s symmetry. The DFT calculated and experimental (FTIR and FT-Raman) wavenumbers and intensities of the normal mode of vibrations and corresponding vibrational assignments for the selected fundamental modes of vibration for the AZT and its charged species are given in Table 2. Experimental wavenumbers and intensities obtained from FTIR (Fig. 2) and FT-Raman (Fig. 3) spectra have been compared with corresponding DFT values (Fig. 4). The frequencies of the amino group appear in the region 3500–3300 cm^{-1} for NH stretching vibrations. The band observed at 3462 cm^{-1} in the FTIR spectrum of the title compound corresponds to the NH stretching vibration of the pyrimidine ring. The assignments agree with the reported results of our previous work on 2-nitroaniline [17]. The DFT calculations for the neutral AZT predict the NH stretching frequency at 3470 cm^{-1} which agrees very well with the experimental data. The DFT calculations for the AZT cation predict the NH stretching frequencies are found to be slightly increased by 4 cm^{-1} after ionization. However, for the AZT anion predicts the frequencies are found to be decreased by 9 cm^{-1}. It can be seen that there is a dramatic increase in the intensity of vibration for this NH stretching mode in the case of AZT cation. The band predicted at 3677 cm^{-1} is due to the OH stretching vibration. But this OH stretching vibrations was not present in both the FTIR and FT-Raman spectra. The DFT calculations for the AZT cation and anion found to be affected and their intensity also drastically changed after ionization. The band observed at 3031–2815 cm^{-1} was due to CH stretching vibrations. The CH stretching vibrations due to pyrimidine ring appears at higher wavenumber 3031 cm^{-1} was assigned which agree with the DFT theoretical value at 3045 cm^{-1}. Also, the CH stretching vibrations due to the presence of furan ring, methyl and methylene group was assigned and their intensity was also analyzed. The C=O stretching was assigned at 1732 and 1722 cm^{-1} in the DFT method, meanwhile in the FTIR and FT-Raman spectra, the assignment goes to 1684 and 1690 cm^{-1} respectively. These assignments were made in analogy with the data predicted by Meenakshi et al. [18]. It is found that the intensity of C=O stretching vibrations of anionic AZT increases drastically more than six times of neutral AZT. The Azide vibrational motions could easily be identified from the infrared spectra [16]. Three characteristic azide vibrational frequencies, including two stretching and one bending modes are listed in Table 3. The DFT calculations predict the peak at 2172, 1287 and 544 cm^{-1} are assigned to asymmetric NNN stretch, symmetric NNN stretching and NNN bending vibrations respectively. The results in the present study are in good agreement with the experimental FTIR and FT-Raman data. It is observed that OH, CH, NH stretching vibrations are slightly decreased in cationic form, whereas these vibrations are slightly increased in anionic form. However, the

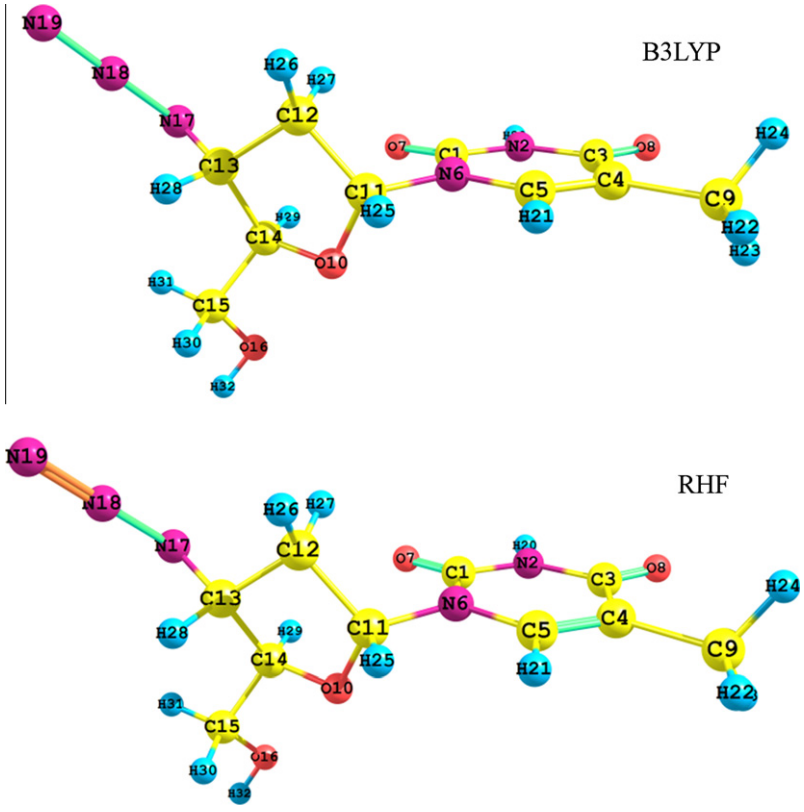

Fig. 1. Optimized geometry of zidovudine.

Table 2
Principal FTIR and FT-Raman and B3LYP wavenumber (cm^{-1}) and their assignments for neutral, cationic and anionic AZT.

S. no	Neutral	Cation	Anion	FTIR	FT-Raman	Assignments
1	3677(21.4)	3685(538.3)	3665(4.3)			O—H stretching
2	3470(67.3)	3474(174.3)	3461(74.7)	3462(s)		N—H stretching
3	3079(7.1)	3090(7.9)	3058(64.0)	3167(m)		CH stretching in pyrimidine ring
4	3045(1.8)	3049(0.4)	3039(4.3)	3031(m)		CH2 stretching in furan ring
5	3008(13.6)	3017(64.2)	2994(25.4)		2988(w)	Asymmetric CH3 stretching in methyl group
6	2986(10.9)	2992(2.2)	2966(32.1)			Asymmetric CH3 stretching in methyl group
7	2972(16.9)	2980(5.0)	2963(18.5)			CH2 stretching in furan ring
8	2966(13.7)	2961(4.1)	2961(39.0)			CH stretching in furan ring
9	2940(28.9)	2950(11.0)	2933(32.2)	2933(m)	2941(w)	CH stretching in furan ring
10	2928(25.0)	2931(70.3)	2913(263.8)			Symmetric CH3 stretching in methyl group
11	2900(31.9)	2908(6.7)	2891(45.3)			CH stretching in furan ring
12	2893(41.2)	2898(34.5)	2879(146.5)			CH2 stretching (a)
13	2857(47.6)	2859(70.0)	2854(18.1)	2817(w)	2815(w)	CH2 stretching (s)
14	2172(655.8)	2129(770.4)	2211(5508.7)	2119(m)		Asymmetric NNN stretching
15	1732(369.5)	1675(53.1)	1753(2005.2)	1684(vs)	1690(w)	C=O stretching
16	1722(847.3)	1631(149.5)	1721(1373.6)			C=O stretching
17	1642(66.0)	1581(1202)	1610(117.0)		1650(vw)	C=C stretching in pyrimidine ring
18	1462(10.2)	1442(18.9)	1464(12.5)	1468(m)		CH2 scissoring
19	1442(48.7)	1430(4.6)	1435(2.8)			CH2 scissoring in furan
20	1287(80.8)	1274(122.7)	1258(37.1)	1284(m)	1280(vw)	Symmetric NNN stretching
21	734(46.2)	727(40.7)	693(7.4)	732(vw)	730(w)	NCO/CCO bending
22	727(14.6)	708(21.8)	677(22.3)	725(vw)	725(w)	NCO/CCO bending
23	544(14.4)	542(13.9)	475(60.8)	540(vw)	548(w)	NNN bending

Inside the parenthesis refers to intensities of the wavenumber.

bending vibrations were decreased in their wavenumber in both cationic and anionic forms.

Frontier molecular orbital analysis

The energies of two important molecular orbitals of AZT, the highest occupied Molecular Orbital (HOMO), and the lowest unoccupied Molecular Orbital (LUMO) were calculated. Fig. 5 shows the HOMO and LUMO of AZT obtained by DFT method. The energy gap between HOMO and LUMO is a critical parameter in determining molecular electrical transport properties [19]. Molecular orbitals (HOMO and LUMO) and their properties such as energy are very useful for physicists and chemists and are very important parameters for quantum chemistry. This is also used by the frontier electron density for predicting the most reactive position in pi-electron systems and also explains several types of reaction in conjugated

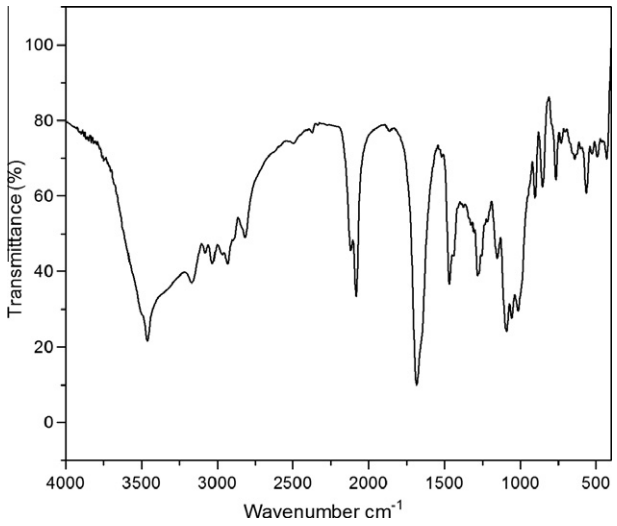

Fig. 2. FTIR spectrum of zidovudine.

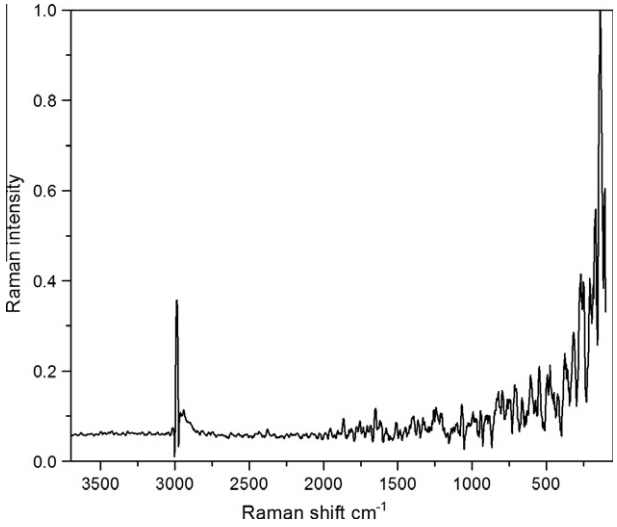

Fig. 3. FT-Raman spectrum of zidovudine.

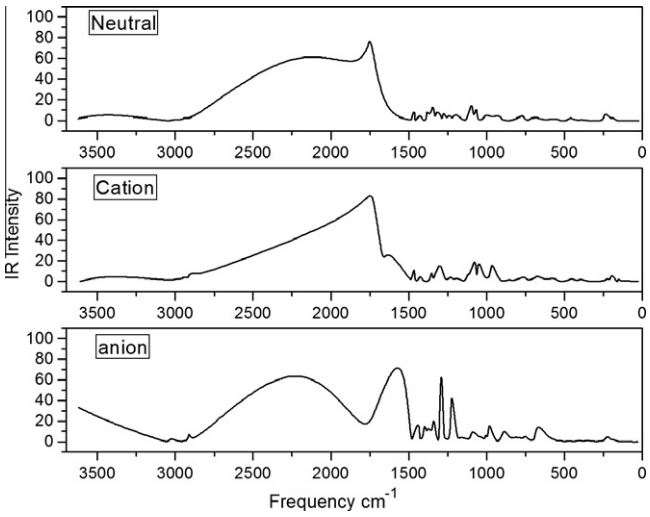

Fig. 4. DFT calculated IR spectrum of zidovudine.

Table 3
Mulliken atomic charges of AZT.

Atom	MPA	
	B3LYP	RHF
C_1	0.7963	0.6541
N_2	−0.6180	−0.5151
C_3	0.5808	0.0824
C_4	−0.0029	0.6552
C_5	0.1166	−0.3957
N_6	−0.5225	0.1318
O_7	−0.5158	−0.4256
O_8	−0.4968	−0.4873
C_9	−0.3591	−0.7497
O_{10}	−0.5043	−0.2130
C_{11}	0.3308	−0.4994
C_{12}	−0.2333	−0.1175
C_{13}	0.0124	−0.2549
C_{14}	0.1941	0.1873
C_{15}	0.0575	−0.3848
O_{16}	−0.5324	−0.4868
N_{17}	−0.3819	0.1888
N_{18}	0.4256	1.0073
N_{19}	−0.2634	−0.9772
H_{20}	0.2906	0.3610
H_{21}	0.1237	0.1682
H_{22}	0.1011	0.1515
H_{23}	0.1394	0.1856
H_{24}	0.1372	0.1839
H_{25}	0.0988	0.0358
H_{26}	0.1154	0.1691
H_{27}	0.1661	0.2566
H_{28}	0.1088	0.1705
H_{29}	0.1515	0.2475
H_{30}	0.0810	0.1403
H_{31}	0.0927	0.1635
H_{32}	0.3096	0.3661

system [20]. The conjugated molecules are characterized by a small highest occupied molecular orbital–lowest unoccupied molecular orbital (HOMO–LUMO) separation, which is the result of a significant degree of intramolecular charge transfer from the end-capping electron-donor groups to the efficient electron-acceptor groups through pi conjugated path leads to the very good for non-linear optical applications [21]. This electronic absorption corresponds to the transition from the ground to the first excited state and is mainly described by one electron excitation from the highest occupied molecular orbital to the lowest unoccupied molecular orbital [22]. Recently, the energy gap between HOMO and LUMO has been used to prove the bioactivity from intramolecular charge transfer [23,24]. The HOMO is located over in both the thymine and furanose ring, the HOMO → LUMO transition implies an electron density transfer from the furanose ring to the fused thymine ring of AZT. Moreover, lower in the HOMO and LUMO energy gap explains the eventual charge transfer interactions taking place within the molecule. The HOMO and LUMO energy calculated by RHF and B3LYP/6-31G∗ method is shown below.

$$\text{HOMO energy} = -9.3548\ \text{a.u. (RHF)\&} - 6.4872\ \text{a.u. (B3LYP)}$$

$$\text{LUMO energy} = 3.2270\ \text{a.u. (RHF)\&} - 1.0520\ \text{a.u. (B3LYP)}$$

$$\text{HOMO} - \text{LUMO energy gap} = 12.58182\ \text{a.u. (RHF)\&5.4352 a.u. (B3LYP)}$$

Atomic charge analysis

The atomic charge in molecules is fundamental to the chemistry. For instance, atomic charge has been used to describe the processes of electronegativity equalization and charge transfer in chemical reactions [25,26]. Mulliken and natural atomic charges

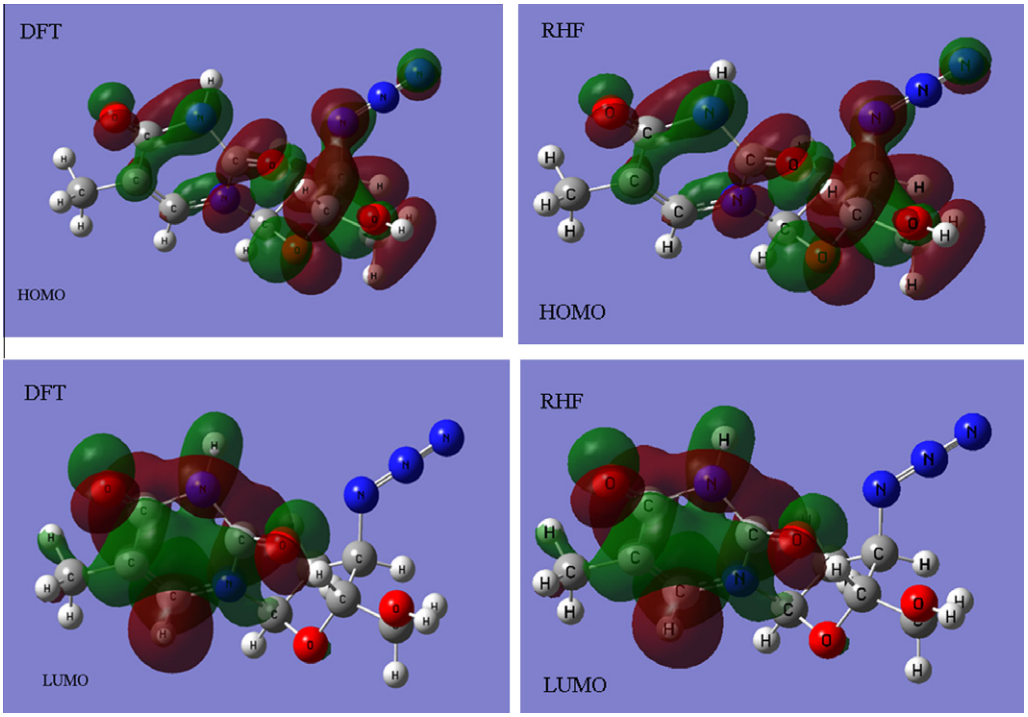

Fig. 5. Frontier molecular orbitals of zidovudine.

calculated at the RHF and B3LYP/6-31G*(d) method is collected in Table 3. It is worthy to mention that electro negative atoms N_2, N_6, O_7, O_8, O_{10}, O_{16}, N_{17} and N_{19} atoms of AZT exhibit negative charge, while N_{18} atom exhibit positive charges. Oxygen O_{16} atom has a maximum negative charge value. The maximum positive atomic charge is obtained for C_1 which is a carbon surrounded by nitrogen and oxygen atoms in the thymine group. The charge on H_{32} and H_{20} atoms has the maximum magnitude of 0.46 and 0.49 respectively among the hydrogen atoms present in the molecule. It is to be noticed that all the hydrogen atoms exhibit a net positive charge. The presence of large negative charge on N and O atom and net positive charge on H atom may suggest the formation of intramolecular interaction and intermolecular transaction through OH and NH bond in solid forms [27].

Chemical reactivity

DFT is one of the important tools of quantum chemistry to understand popular chemical concepts such as electronegativity, electron affinity, chemical potential and ionization potential [28]. The electron density-based local reactivity descriptors such as Fukui functions were proposed to explain the chemical selectivity or reactivity at a particular site of a chemical system [29]. Electron density is a property that contains all the information about the molecular system and plays an important role in calculating almost all these chemical quantities. Parr and Yang [30] proposed a finite difference approach to calculate Fukui function indices, i.e. nucleophilic, electrophilic and radical attacks. In order to solve the negative Fukui function problem, different attempts have been made by various groups [31–33]. Kolandaivel et al. [34] introduced the atomic descriptor to determine the local reactive sites of the molecular system. In the present study, the optimized molecular geometry was utilized in single-point energy calculations, which have been performed at the DFT for the anions and cations of the conformers using the ground state with doublet multiplicity. The individual atomic charges calculated by Mulliken population analysis (MPA) have been used to calculate the Fukui function. Table 4 shows the f_k and $(sf)_k$ values for the AZT. From the tables one can find that the complexities associated with f_k values due to the negative values being removed in the $(sf)_k$ values. In order to confirm that the atomic descriptor would produce the reactive sites without disturbing the trend, we have performed the calculation for the reactive sites of the stable structures of AZT. It has been found that the MPA schemes predict N19 has higher f_k^+ value indicates the possible site for nucleophilic attack. The observed nucleophilicity trend in all the conformers is N19 > O8 > O7. The observation of the reactive sites by $(sf)_k$ is found almost identical to f_k Even though the $(sf)_k$ values are numerically less it should be worth noting that the values are positive and the ordering of the reactivity has not been changed in any cases. The calculated f_k^- value predicts that the possible site for electrophillic attack is N19 and C6 site.

Table 4
Condensed Fukui function f_k and descriptors $(sf)_k$ (10^{-2}) for AZT.

Atom	f_k^+	f_k^-	$(sf)_k^+$	$(sf)_k^-$
C_1	0.0293	0.0278	0.0158	0.0142
N_2	−0.0018	0.0025	0.0001	0.0001
C_3	0.0365	0.0808	0.0245	0.1202
C_4	0.0397	0.0005	0.0290	0.0000
C_5	0.0389	0.0935	0.0278	0.1607
N_6	0.0437	−0.0091	0.0352	0.0015
O_7	0.0718	0.0379	0.0950	0.0264
O_8	0.0874	0.0886	0.1406	0.1445
C_9	−0.0157	−0.0086	0.0046	0.0013
O_{10}	0.0335	0.0148	0.0206	0.0040
C_{11}	−0.0183	−0.0112	0.0061	0.0023
C_{12}	−0.0142	−0.0120	0.0037	0.0027
C_{13}	−0.0137	−0.0330	0.0035	0.0200
C_{14}	−0.0202	−0.0110	0.0075	0.0022
C_{15}	−0.0052	0.0052	0.0005	0.0005
O_{16}	0.0276	0.0034	0.0140	0.0002
N_{17}	0.0472	0.0590	0.0410	0.0641
N_{18}	0.0233	0.0894	0.0100	0.1471
N_{19}	0.0983	0.1569	0.1780	0.4532

Conclusion

In this study, the spectroscopic properties of the compound were examined by FTIR and FT-Raman techniques. The FT-IR and FT-Raman spectral measurements have been made for the zidovudine. Various quantum chemical calculations help us to identify the structural and symmetry properties of the molecule. The comparative result of experimental and theoretical study gave us a full description of the geometry and vibrational properties of title molecule. Mulliken atomic charges of the title molecule have been studied by both the HF and DFT methods. The consistency between the calculated and experimental FT-IR and FT-Raman data indicates that the B3LYP/6-31G(d,p) method can generates reliable geometry and related properties of the title compound. Charge transfer occurs in the molecule between HOMO and LUMO energies, and frontier energy gap are calculated and presented.

References

[1] F.X. Zhou, Z.K. Liao, J. Dai, J. Xiong, C.H. Xie, Z.G. Luo, S.Q. Liu, Y.F. Zhou, Radio sensitization effect of zidovudine on human malignant glioma cells, Biochem. Biophys. Res. Commun. 354 (2007) 351–356.

[2] R. Yarchoan, H. Mitsuya, S. Broder, AIDS therapies, Sci. Am. 259 (4) (1988) 110–119.

[3] I.D. Dyer, J.N. Low, P.T. Tollin, H.R. Wilson, Alan Howie, Acta Crystal C44 (1988) 767–769.

[4] F. Cheng, L. Selvam, F. Wang, Blue shifted intramolecular C—H···O improper hydrogen bonds in conformers of zidovudine, Chem. Phys. Lett. 493 (2010) 358–363.

[5] A. Peepliwal, S.D. Vyawahare, C.G. Bonde, A quantitative analysis of zidovudine containing formulation by FT-IR and UV spectroscopy, Anal. Methods 2 (2010) 1756–1763.

[6] U.Y. Nayak, S. Gopal, S. Mutalik, A.K. Ranjith, M.S. Reddy, P. Gupta, N. Udupa, Glutaraldehyde cross-linked chitosan microspheres for controlled delivery of zidovudine, J. Microencapsul. 26 (2009) 214–222.

[7] L. Rivas, S. Sanchez-Cortes, J.V. Garcıa-Ramos, Conformational study of AZT in aqueous solution and adsorbed on a silver surface by means of Raman spectroscopy, J. Raman Spect. 33 (2001) 6–9.

[8] L. Rivas, S. Sanchez-Corte, J.V. Garcıa-Ramos, Raman structural study of thymine and its 20-deoxy-ribosyl derivatives in solid state aqueous solution and when adsorbed on silver nanoparticles, Phys. Chem. Chem. Phys. 4 (2002) 1943–1948.

[9] M.A. Raviolo, P.A.M. Williams, S.B. Etcheverry, O.E. Piro, E.E. Castellano, M.S. Gualdesi, M.C. Briñón, Synthesis molecular structure and physicochemical properties of bis(3_-azido-3_-deoxythymidin-5_-yl) carbonate, J. Mol. Struct. 970 (2010) 59–65.

[10] H. Kruszewska, U. Chmielowiec, E. Bednarek, J. Witowska-Jarosz, J.C. Dobrowolski, A. Misicka, Spectroscopic identification of AZT derivative obtained from biotransformation of AZT by *Stenotrophomonas maltophilia*, J. Mol. Struct. 651–653 (2003) 645–650.

[11] M.J. Frisch, G.W. Trucks, H.B. Schlegel, G.E. Scuseria, M.A. Robb, J.R. Cheeseman, G. Scalmani, V. Barone, B. Mennucci, G.A. Petersson, H. Nakatsuji, M. Caricato, X. Li, H.P. Hratchian, A.F. Izmaylov, J. Bloino, G. Zheng, J.L. Sonnenberg, M. Hada, M. Ehara, K. Toyota, R. Fukuda, J. Hasegawa, M. Ishida, T. Nakajima, Y. Honda, O. Kitao, H. Nakai, T. Vreven, J.A. Montgomery, Jr. J.E. Peralta, F. Ogliaro, M. Bearpark, J.J. Heyd, E. Brothers, K.N. Kudin, V.N. Staroverov, R. Kobayashi, J. Normand, K. Raghavachari, A. Rendell, J.C. Burant, S.S. Iyengar, J. Tomasi, M. Cossi, N. Rega, J.M. Millam, M. Klene, J.E. Knox, J.B. Cross, V. Bakken, C. Adamo, J. Jaramillo, R. Gomperts, R.E. Stratmann, O. Yazyev, A.J. Austin, R. Cammi, C. Pomelli, J.W. Ochterski, R.L. Martin, K. Morokuma, V.G. Zakrzewski, G.A. Voth, P. Salvador, J.J. Dannenberg, S. Dapprich, A.D. Daniels, O. Farkas, J.B. Foresman, J.V. Ortiz, J. Cioslowski, D.J. Fox, Gaussian, Inc., Wallingford CT, 2009.

[12] D. Becke, J. Chem. Phys. 98 (1993) 5648–5652.

[13] C. Lee, W. Yang, R.G. Parr, Phys. Rev. B 37 (1988) 785–789.

[14] H.B. Schlegel, J. Comput. Chem. 3 (1982) 214–218.

[15] H.B. Schlegel, J. Chem. Phys. 77 (1982) 3676–3681.

[16] Fang-Fang. Che, Feng. Wang, Electronic structure of the azide group in 3′-azido-3′- deoxythymidine (AZT) compared to small azide compounds, Molecules 14 (2009) 2656–2668.

[17] S. Azhagiri, G.R. Ramkumaar, S. Jayakumar, S. Kumaresan, R. Arun, S. Gunasekaran, S. Srinivasan, Theoretical and experimental studies of vibrational spectra and thermal analysis of 2-nitroaniline and its cation, J. Mol. Model. 16 (2010) 87–94.

[18] R. Meenakshi, L. Jaganathan, S. Gunasekaran, S. Srinivasan, Density functional theory restricted Hartree–Fock simulations and vibrational spectroscopic studies of nicorandil, Mol. Simul. 36 (6) (2010) 425–433.

[19] K. Fukui, Science 218 (1982) 747–754.

[20] K. Fukui, T. Yonezawa, H. Shingu, Chem. J. Phys. 20 (1952) 722–725.

[21] C.H. Choi, M. Kertesz, Chem. J. Phys. 101A (1997) 3823–3831.

[22] M. Kurt, P. ChinnaBabu, N. Sundaraganesan, M. Cinar, M. Karabacak, Spectrochim. Acta Part A 79 (2011) 1162–1170.

[23] L. Padmaja, C. Ravikumar, D. Sajan, I.H. Joe, V.S. Jayakumar, G.R. Pettit, O.F. Nielsen, J. Raman Spectrosc. 40 (2009) 419–428.

[24] C. Ravikumar, I.H. Joe, V.S. Jayakumar, Chem. Phys. Lett. 460 (2008) 552–558.

[25] K. Jug, Z.B. Maksic, in: Z.B. Maksic (Ed.), Theoretical Model of Chemical Bonding, Part 3, Springer, Berlin, 1991, p. 233.

[26] S. Fliszar, Charge Distributions and Chemical Effects, Springer, New York, 1983.

[27] L. Xiao-Hong et al., Comput. Theor. Chem. 969 (2011) 27–34.

[28] P. Hohenberg, W. Kohn, Inhomogenous electron gas, Phys. Rev. 136 (1964) B864–B871.

[29] W. Yang, R.G. Parr, Hardness softness and the fukui function in the electronic theory of metals and catalysis, Proc. Natl Acad. Sci. USA 82 (1985) 6723–6726.

[30] R.G. Parr, W. Yang, Density functional approach to the frontierelectron theory of chemical reactivity, J. Am. Chem. Soc. 106 (1984) 4049–4050.

[31] R.K. Roy, K. Hirao, S. Krishnamurthy, S. Pal, Mulliken population analysis based evaluation of condensed Fukui function indices using fractional molecular charge, J. Chem. Phys. 115 (2001) 2901–2907.

[32] P. Bultinck, R. Carbo-Dorca, W. Langenaekar, Negative Fukui functions: new insights based on electronegativity equalization, J. Chem. Phys. 118 (2003) 4349–4356.

[33] P. Butlinck, R. Carbo-Dorca, Negative and infinite Fukui functions: the role of diagonal dominance in the hardness matrix, J. Math. Chem. 34 (2003) 67–74.

[34] P. Kolandaivel, G. Praveen, P. Selvarengan, Study of atomic and condensed atomic indices for reactive sites of molecules, J. Chem. Sci. 117 (5) (2005) 591–598.